High-Pressure, Low-Temperature, Single-Crystal Neutron Diffraction Study of Deuterated and Hydrogenous Ammonium Hexaaquacopper(II) Sulfate (Tutton's Salt): A Pressure-Switchable Jahn-Teller Distortion

Charles J. Simmons,*,† Michael A. Hitchman,*,‡ Horst Stratemeier,‡ and Arthur J. Schultz*,§

Contribution from the Mathematics and Science Division, Brigham Young University—Hawaii, Laie, Hawaii 96762, Department of Chemistry, University of Tasmania, Box 252 C, Hobart, Tasmania 7001, Australia, and Chemistry and Materials Science Divisions, Argonne National Laboratory, Argonne, Illinois 60439

Received March 12, 1993. Revised Manuscript Received August 16, 1993®

Abstract: The first example of a pressure-induced Jahn-Teller distortion switch has been observed in a single-crystal time-of-flight neutron diffraction study of the Tutton salt $(ND_4)_2[Cu(D_2O)_6](SO_4)_2$ at $T = 15$ K, $P = 1$ bar ($\mathbf{D_L}$) and $T = 15$ K, $P = 1.5$ kbar ($\mathbf{D_H}$). Also studied was the hydrogenous salt $(NH_4)_2[Cu(H_2O)_6](SO_4)_2$ at $T = 14$ K, $P = 1.4$ kbar ($\mathbf{H_H}$). The unit cell parameters are as follows: $\mathbf{D_L}$, $a = 9.451(2)$ Å, $b = 12.736(3)$ Å, $c = 6.096(1)$ Å, $\beta = 107.13(2)°$, $Z = 2$, $V = 701.2(3)$ Å^3, space group = $P2_1/a$; $\mathbf{D_H}$, $a = 9.136(1)$ Å, $b = 12.285(2)$ Å, $c = 6.371(1)$ Å, $\beta = 106.28(2)°$, $Z = 2$, $V = 686.4(2)$ Å^3, space group = $P2_1/a$; $\mathbf{H_H}$, $a = 9.068(2)$ Å, $b = 12.232(2)$ Å, $c = 6.340(1)$ Å, $\beta = 106.44(2)$, $Z = 2$, $V = 674.5(2)$ Å^3, space group = $P2_1/a$. Application of 1.5 kbar of pressure to the deuterated crystal produces a decrease in the lengths of the a and b axes by 0.315(2) and 0.451(4) Å, respectively, whereas the c axis increases by 0.275(1) Å. Comparison of the $\mathbf{D_L}$ and $\mathbf{D_H}$ structures shows that the long axis of the Jahn-Teller distortion has switched by 90°, i.e., Cu(1)–O(7) = 2.022(2) and Cu(1)–O(8) = 2.310(2) Å for $\mathbf{D_L}$ vs Cu(1)–O(7) = 2.290(2) and Cu(1)–O(8) = 2.014(2) Å for $\mathbf{D_H}$, so that the $\mathbf{D_H}$ and $\mathbf{H_H}$ structures are similar. For $\mathbf{H_H}$ Cu(1)–O(7) = 2.272(2) and Cu(1)–O(8) = 2.005(2) Å. The switching of the long axis of the Jahn-Teller distortion appears to be associated with the rotation of the ND_4^+ ion with a concomitant change in the hydrogen bonding of the coordinated water molecules with the SO_4^{2-} ions. The resulting adiabatic potential energy surfaces are calculated using tetragonal and orthorhombic strain parameters estimated from the temperature variation of the Cu–O bond lengths.

Introduction

The Jahn-Teller theorem has proven extremely useful in the interpretation of many aspects of the behavior of a range of transition-metal compounds.[1] In particular, it has provided the framework within which the stereochemistry and spectroscopic properties of Cu^{2+} complexes are generally interpreted, and interest in this area has increased recently with the suggestion that Jahn-Teller coupling may play a role in the mechanism underlying the behavior of the so-called "warm" superconductors.[2]

An unusual feature of copper(II) stereochemistry is the fact that the geometry and electronic structure of many complexes are temperature dependent.[3] Following the pioneering work by Bleaney and co-workers on the $Cu(H_2O)_6^{2+}$ ion in Cu^{2+}-doped $[Zn(H_2O)_6]SiF_6$,[4] this aspect has been studied by EPR spectroscopy in a range of compounds,[5-10] and a theoretical model which interprets the temperature-dependent g values of six-coordinate copper(II) compounds in terms of Jahn-Teller coupling and the influence of nonequivalent ligands was described recently.[8-10] These spectroscopic studies have concentrated largely on the complexes formed when Cu^{2+} is doped into diamagnetic host lattices, but similar conclusions have been drawn from investigations of the way in which crystal structures of a range of complexes of general formula $[Cu(diamine)_2O_2X]^+$ change as a function of temperature, where O_2X is a bidentate oxygen donor ligand.[11,12]

Particular interest has been shown in the isomorphous series of Tutton salts, of general formula $(cation)_2[M(H_2O)_6](SO_4)_2$, where M is a divalent metal ion. The "fluxional" behavior of the $Cu(H_2O)_6^{2+}$ group in several of the complexes has been studied by EPR spectroscopy,[5,6,9] while the charge density in $(NH_4)_2[Cr(H_2O)_6](SO_4)_2$ and its deuterated analog, which resemble the copper(II) compounds in that the high-spin Cr^{2+} ion is expected to be subject to strong Jahn-Teller coupling, has been the subject of detailed analysis at low temperature by X-ray and neutron diffraction.[13] A novel feature of the chromium(II) complex is the observation[14] that, in mixed crystals formed with the isostructural zinc(II) compound, the direction of the long Cr–O bonds of the Jahn-Teller distorted $Cr(H_2O)_6^{2+}$ complex depends upon the Cr/Zn ratio.

† Brigham Young University.
‡ University of Tasmania.
§ Argonne National Laboratory.
® Abstract published in *Advance ACS Abstracts*, October 1, 1993.

(1) See, for example: Bersuker, I. B. *The Jahn-Teller Effect and Vibronic Interactions in Modern Chemistry*; Plenum Press: New York, 1983.
(2) Fil, D. V.; Tokar, O. I.; Shelankov, A. L.; Weber, W. *Phys. Rev. B* **1992**, *45*, 5633 and references therein.
(3) Gazo, J.; Bersuker, I. B.; Garaj, J.; Kabesova, M.; Kohout, J.; Langfelderova, H.; Melnik, M.; Serator, M.; Valach, F. *Coord. Chem. Rev.* **1976**, *11*, 253.
(4) Bleaney, B.; Ingram, D. J. E. *Proc. Phys. Soc., London, Sect. A* **1950**, *63*, 408.
(5) Silver, B. L.; Getz, D. *J. Chem. Phys.* **1974**, *61*, 638.
(6) Petrashen, V. E.; Yablokov, Yu. V.; Davidovitch, R. L. *Phys. Status Solidi B* **1980**, *101*, 117.
(7) Zaitdinov, A. M.; Davidovitch, R. L.; Ya Shevshenko, V.; Yablokov, Yu. V. *Koord. Khim.* **1982**, *9*, 1644.
(8) Riley, M. J.; Hitchman, M. A.; Reinen, D. *Chem. Phys.* **1986**, *102*, 11.
(9) Riley, M. J.; Hitchman, M. A.; Wan Mohammed, A. *J. Chem. Phys.* **1987**, *87*, 3766.
(10) Riley, M. J.; Hitchman, M. A.; Reinen, D.; Steffen, G. *Inorg. Chem.* **1988**, *27*, 1924.
(11) Simmons, C. J.; Hathaway, B. J.; Amornjarusiri, K.; Santasiero, B. D.; Clearfield, A. *J. Am. Chem. Soc.* **1987**, *109*, 1947.
(12) Stebler, M.; Bürgi, H. B. *J. Am. Chem. Soc.* **1987**, *109*, 1395.
(13) Figgis, B. N.; Kucharski, E. S.; Reynolds, P. A. *Acta Crystallogr.* **1990**, *B46*, 577. Figgis, B. N.; Kucharski, E. S.; Forsyth, J. B. *Acta Crystallogr.* **1991**, *C47*, 419.
(14) Cotton, F. A.; Falvello, L.; Murillo, C. Private communication.

0002-7863/93/1515-11304$04.00/0

Table I. Unit Cell, Data Collection, and Refinement Parameters

	$(ND_4)_2[Cu(D_2O)_6](SO_4)_2$	$(ND_4)[Cu(D_2O)_6](SO_4)_2$	$(NH_4)_2[Cu(H_2O)_6](SO_4)_2$
temp (K)	15	15	14
Pressure	1 bar	1.5 kbar	1.4 kbar
shorthand designation	D_L	D_H	H_H
space group		monoclinic $P2_1/a$	
Z		2 formula units per unit cell	
a (Å)	9.451(2)	9.136(1)	9.068(2)
b (Å)	12.736(3)	12.285(2)	12.232(2)
c (Å)	6.096(1)	6.371(1)	6.340(1)
β (deg)	107.13(2)	106.28(2)	106.44(2)
V (Å^3)	701.2(3)	686.4(2)	674.5(2)
radiation		neutrons	
wavelenth range		λ = 0.7–4.2 Å determned by time-of-flight	
data colln technique		time-of-flight Laue with 30 × 30 cm^2 position-sensitive detector	
linear abs coeff, μ (cm^{-1})		$0.240 \pm 0.016\lambda$	$1.226 + 1.163\lambda$
spherical abs corr radius, r (cm)		0.10	0.10
extinction param g (rad^{-1} × 10^{-4})	0.095(5)	0.077(4)	0.053(4)
no. of refls in final l.s. ($F^2 > 5\sigma$)	1328	1235	1892
no. of unique refls	1002	870	1327
function minimized		$\sum w(\|F_o\| - \|F_c\|)^2$	
$R(F)$	0.050	0.041	0.050
$R_w(F)$	0.052	0.043	0.048
GOF	1.53	1.15	1.35

The first three-dimensional single-crystal X-ray structure of the Tutton salt $(NH_4)_2[Cu(H_2O)_6](SO_4)_2$, derived from film measurements at room temperature, was reported in 1966[15] and was followed in 1969 by a more precise room-temperature single-crystal neutron study[16] from which the hydrogen atoms were also accurately located. The coordination about the copper atom, which is located on a center of symmetry in these structures, was shown to have a rhombic distortion, with distances of Cu–O(7) = 2.230(1), Cu–O(8) = 2.073(1), and Cu–O(9) = 1.966(1) Å. A particular point of interest is that in all of the isomorphous alkali metal salts $A_2[Cu(H_2O)_6](SO_4)_2$ (A = K, Rb, Cs)[17,18] the Cu–O(7) and Cu–O(8) distances are switched, such that Cu–O(7) = 2.03, Cu–O(8) = 2.30, and Cu–O(9) = 1.96 Å.

In 1984, Hathaway and Hewat reported the neutron powder structure of the deuterated salt $(ND_4)_2[Cu(D_2O)_6](SO_4)_2$ at seven different temperatures between 5 and 295 K.[19a] One of the most interesting findings of this study was a structural isotope effect in which the long axis of the Jahn–Teller distortion had switched compared with that found in the hydrogenous ammonium salt. It was also observed that the Cu–O(7) and Cu–O(8) bond lengths appear to vary with temperature, which is consistent with a dynamic equilibrium between forms in which the long axis of the Jahn–Teller distortion switches between these two bonds. In the same year, the single-crystal X-ray structure of the hydrogenous salt was examined at 203 and 123 K.[18] On the basis of X-ray data and variable-temperature EPR data, it was concluded that the CuO_6 chromophore in this salt is fluxional and is changing dynamically between two different structures with an energy difference ΔE of ca. 160 cm^{-1}. Behavior of this kind has also been established in several studies of the temperature dependence of the EPR spectra of Cu^{2+} doped into a range of Tutton salts.[5,6,9] In 1988, room-temperature single-crystal X-ray and neutron data were used in an analysis of the deformation density in the Cu–O bonds and of the role of the hydrogen bonds in differentiating the Cu–O(7) and Cu–O(8) bonds.[20] Very recently, the structure of the deuterated compound was determined at 85 K by X-ray diffraction,[19b] and the charge density distribution about the Cu^{2+} ion was deduced.

In this paper, we report the single-crystal time-of-flight neutron diffraction structures of the deuterated salt at 15 K and ambient pressure (1 bar) and at 15 K and 1.5 kbar. We also present the structure of the hydrogenous salt at 14 K and 1.4 kbar. As will be described, the application of pressure on the deuterated crystal results in a switch of the Jahn–Teller distortion, such that the high-pressure deuterated structure is isomorphous with the hydrogenous salt but not with the alkali metal salts. The structural changes are discussed in terms of the effects of lattice strain interactions upon the Jahn–Teller potential energy surface of the $Cu(D_2O)_6^{2+}$ and $Cu(H_2O)_6^{2+}$ complexes.

Experimental Section

Synthesis of $(ND_4)_2[Cu(D_2O)_6](SO_4)_2$ and $(NH_4)_2[Cu(H_2O)_6](SO_4)_2$. Crystals of $(ND_4)_2[Cu(D_2O)_6](SO_4)_2$ were grown by dissolving anhydrous $CuSO_4$ (0.79 g) and dried $(NH_4)_2SO_4$ (0.65 g) in 10 mL of D_2O and allowing the solution to evaporate almost to dryness in a desiccator over silica gel. The crude material was recrystallized twice by dissolving it in 10 mL of D_2O and allowing it to evaporate almost to dryness in a desiccator. Crystals of $(NH_4)_2[Cu(H_2O)_6](SO_4)_2$ were grown by slowly evaporating an aqueous solution of an equimolar mixture of $CuSO_4 \cdot 5H_2O$ and $(NH_4)_2SO_4$.

Neutron Data Collection. Time-of-flight neutron data were obtained at the Intense Pulsed Neutron Source (IPNS) at Argonne National Laboratory using the single-crystal diffractometer equipped with a position-sensitive ^{6}Li-glass scintillation area (30 × 30 cm^2) detector.[21] At the IPNS, pulses of protons are accelerated into a heavy-element target 30 times a second to produce pulses of neutrons by the spallation process. Because of the pulsed nature of the source, neutron wavelengths are determined by time-of-flight on the basis of the de Broglie equation $\lambda = (h/m)(t/l)$, where h is Planck's constant, m is the neutron mass, and t is the time-of-flight for a flight path l, so that the entire thermal spectrum of neutrons can be used. With an area position-sensitive detector and a range of neutron wavelengths, a solid volume of reciprocal space is sampled with a stationary orientation of the sample and the detector. Details of the data collection and analysis procedures have been previously provided.[22,23] Table I contains a summary of the data collection, analysis, and refinement parameters for this experiment.

Temperature and pressure were controlled using a helium gas pressure cell mounted on the cold stage of a Displex closed-cycle helium refrigerator (Air Products and Chemicals, Inc., Model CS-202). Crystals in the pressure cell were immersed in the fluorinated hydrocarbon Fluorinert (3M Co.) in order to provide hydrostatic pressure conditions. For the

(15) Montgomery, H.; Lingafelter, E. *Acta Crystallogr.* **1966**, *20*, 659.
(16) Brown, G. M.; Chidambaram, R. *Acta Crystallogr., Sect. B* **1969**, *25*, 676.
(17) Hathaway, B. J. *Struct. Bonding* **1984**, *57*, 55.
(18) Alcock, N. W.; Duggan, M.; Murray, A.; Tyagi, S.; Hathaway, B. J.; Hewat, A. W. *J. Chem. Soc., Dalton Trans.* **1984**, 7.
(19) (a) Hathaway, B. J.; Hewat, A. W. *J. Solid State Chem.* **1984**, *51*, 364. (b) Figgis, B. N.; Khor, L.; Kucharski, E. S.; Reynolds, P. A. *Acta Crystallogr.* **1992**, *B48*, 144.
(20) Maslen, E. N.; Watson, K. J.; Moore, F. H. *Acta Crystallogr.* **1988**, *B44*, 102.
(21) Schultz, A. J. *Trans. Am. Crystallogr. Assoc.* **1987**, *23*, 61.
(22) Schultz, A. J.; Srinivasan, K.; Teller, R. G.; Williams, J. M.; Lukehart, C. M. *J. Am. Chem. Soc.* **1984**, *106*, 999.
(23) Schultz, A. J.; Van Derveer, D. G.; Parker, D. W.; Baldwin, J. E. *Acta Crystallogr.* **1990**, *C46*, 276.

deuterated sample, the crystal was sealed in the pressure cell at room temperature and ambient pressure and then cooled to 15 K for the low pressure (≈1 bar) data collection. Following completion of the low-pressure data collection, the crystal was warmed to room temperature, pressurized to 1.5 kbar, and cooled back to 15 K for the high-pressure data collection.

For each of the two crystals, an orientation matrix was initially obtained by an auto-indexing procedure[24] using data obtained by searching a histogram for peaks. For the $\mathbf{D_L}$ (deuterated, low pressure), $\mathbf{D_H}$ (deuterated, high pressure), and $\mathbf{H_H}$ (hydrogenous, high pressure) data collections, 15, 18, and 24 diffractometer settings, respectively, were used to obtain at least one unique quadrant of reciprocal space plus some additional equivalent data in some cases. For each setting of the diffractometer angles, data were stored in three-dimensional histogram form with coordinates x, y, and t corresponding to the horizontal and vertical detector positions and the time-of-flight, respectively. The 120 time-of-flight histogram channels were constructed with constant $\Delta t/t = 0.015$ and correspond to wavelengths of 0.7–4.2 Å. Bragg reflections were integrated about their predicted locations and were corrected for the Lorentz factor, the incident spectrum, the detector efficiency, and dead-time losses. A wavelength-dependent spherical absorption correction was applied.[25] Symmetry-related reflections were not averaged since different extinction factors were applicable to reflections measured at different wavelengths. Unit cell parameters in Table I were obtained from a least-squares refinement of the observed centroid positions of the strongest peaks from each set of data (928, 1072, and 1958 for $\mathbf{D_L}$, $\mathbf{D_H}$, and $\mathbf{H_H}$, respectively).

Solutions and Refinements of the Structures. The initial atomic positional coordinates for the $\mathbf{D_L}$ structure were obtained from the neutron powder analysis by Hathaway and Hewat.[19a] In the case of the $\mathbf{D_H}$ structure, initial attempts to refine a model based on the $\mathbf{D_L}$ structure were unsuccessful. Although the unusual change in the unit cell parameters (see Table I) to those resembling the hydrogenous crystal should have led us to try that as a starting model, we instead resorted to direct methods to solve the structure. Using MULTAN80,[26] the coordinates of the copper and the three coordinated oxygen atoms were obtained. Refinement of the 18 scale factors (one for each histogram of data) gave $R_w(F) = 0.66$, but subsequent series of difference Fouriers and refinements led to the location of all of the atoms. To our knowledge, there are only two other single-crystal structures solved by direct methods from time-of-flight neutron diffraction data.[27,28] Finally, the starting model for the $\mathbf{H_H}$ structure was that for $\mathbf{D_H}$.

For all three structures, atomic scattering lengths used in the least-squares refinements were those tabulated by Sears[29] ($b_{Cu} = 0.7718$, $b_S = 0.2847$, $b_O = 0.5803$, $b_N = 0.936$, $b_H = -0.3739$, and $b_D = 0.6671$, all in units of 10^{-12} cm). In the final cycles of least-squares refinements, all hydrogen atoms were treated with anisotropic temperature factors and a secondary extinction correction (Becker and Coppens formalism,[30] type I, Lorentzian distribution) was included. Due to the small observations-to-parameters ratios, all the non-hydrogen atoms, which have small thermal displacements at low temperatures, were refined isotropically in the final cycles. Table II contains the final atomic coordinates and isotropic temperature factors. Interatomic distances and angles are given in Table III. Anisotropic temperature factors and observed and calculated structure factors are given as supplementary material.

Results and Discussion

Crystal Structures. The single-crystal structure of $(ND_4)_2[Cu(D_2O)_6](SO_4)_2$ at 15 K and 1 bar, shown in Figures 1a, 2a, and 3a, is in good agreement with those of Hathaway and Hewat[19a] derived from neutron powder diffraction data at 5 K and of Figgis et al.[19b] derived from single-crystal X-ray diffraction data at 85 K. The unit cell parameters obtained from the present data are 0.02–0.03 Å longer than those for the other studies, apparently due to systematic errors associated with the use of the pressure cell which may introduce crystal alignment errors. Bond lengths for the three structures agree to within 0.01–0.02 Å with those obtained by Hathaway and Hewat and by Figgis et al., which is generally in the range of three standard deviations.

The application of 1.5 kbar of pressure to the deuterated crystal produces a decrease in the lengths of the a and b axes by 0.315(2)

Table II. Atomic Positional and Isotropic or Equivalent Isotropic Thermal Parameters[a]

atom	x	y	z	U_{iso} or U_{eq} (Å^2)
Cu(1)	0.0	0.0	0.0	0.0013(4)
	0.0	0.0	0.0	0.0003(4)
	0.0	0.0	0.0	0.0055(3)
S(2)	0.3870(4)	0.1441(3)	0.7479(9)	0.0003(7)
	0.4204(5)	0.1347(3)	0.7439(8)	0.0011(7)
	0.4199(4)	0.1342(3)	0.7425(6)	0.0059(5)
O(3)	0.3805(2)	0.2386(2)	0.6059(5)	0.0032(4)
	0.4310(3)	0.2274(2)	0.5954(4)	0.0030(4)
	0.4309(2)	0.2271(1)	0.5961(3)	0.0078(3)
O(4)	0.5277(2)	0.0871(2)	0.7755(5)	0.0039(4)
	0.5579(2)	0.0660(2)	0.7826(4)	0.0038(4)
	0.5581(2)	0.0662(1)	0.7833(3)	0.0089(3)
O(5)	0.2609(2)	0.0728(2)	0.6302(4)	0.0025(4)
	0.2831(2)	0.0682(2)	0.6304(4)	0.0031(3)
	0.2837(2)	0.0682(1)	0.6313(3)	0.0078(3)
O(6)	0.3730(2)	0.1734(2)	0.9785(5)	0.0037(4)
	0.4018(2)	0.1787(2)	0.9509(4)	0.0030(4)
	0.4026(2)	0.1790(1)	0.9521(3)	0.0073(3)
O(7)	0.1512(2)	0.1077(2)	0.1649(5)	0.0039(4)
	0.1868(2)	0.1190(2)	0.1772(4)	0.0042(4)
	0.1868(2)	0.1188(1)	0.1771(3)	0.0093(3)
O(8)	−0.1805(2)	0.1118(2)	0.0502(5)	0.0033(4)
	−0.1570(2)	0.1095(2)	0.0298(4)	0.0031(4)
	−0.1578(2)	0.1092(1)	0.0294(3)	0.0075(3)
O(9)	0.0109(2)	−0.0661(2)	0.2960(5)	0.0028(4)
	−0.0051(2)	−0.0638(2)	0.2846(4)	0.0031(3)
	−0.0053(2)	−0.0645(1)	0.2840(3)	0.0080(3)
N(10)	0.1265(1)	0.3645(1)	0.3775(3)	0.0041(3)
	0.1431(2)	0.3413(1)	0.3575(3)	0.0047(3)
	0.1427(1)	0.34165(9)	0.3581(2)	0.0091(2)
D(11)	0.0422(3)	0.3463(2)	0.2309(5)	0.0207(9)[b]
D(11)	0.0800(3)	0.3278(3)	0.1995(5)	0.0223(9)[b]
H(11)	0.0803(5)	0.3271(3)	0.1998(6)	0.030(1)[b]
D(12)	0.2043(3)	0.3062(2)	0.4214(6)	0.0201(8)[b]
D(12)	0.2398(3)	0.2942(2)	0.3973(6)	0.0213(9)[b]
H(12)	0.2395(4)	0.2948(3)	0.3975(8)	0.030(1)[b]
D(13)	0.0834(3)	0.3775(2)	0.5115(6)	0.0196(8)[b]
D(13)	0.0757(3)	0.3198(2)	0.4570(5)	0.0192(8)[b]
H(13)	0.0767(5)	0.3206(3)	0.4590(7)	0.026(1)[b]
D(14)	0.1773(3)	0.4329(2)	0.3516(6)	0.0204(9)[b]
D(14)	0.1707(3)	0.4234(2)	0.3743(6)	0.0201(8)[b]
H(14)	0.1708(4)	0.4242(3)	0.3740(7)	0.026(1)[b]
D(15)	0.1961(3)	0.0929(2)	0.3294(5)	0.0181(8)[b]
D(15)	0.2322(3)	0.0941(2)	0.3264(5)	0.0194(8)[b]
H(15)	0.2315(4)	0.0943(3)	0.3266(6)	0.025(1)[b]
D(16)	0.2311(3)	0.1257(2)	0.0989(5)	0.0188(8)[b]
D(16)	0.2705(3)	0.1263(2)	0.1095(5)	0.0197(8)[b]
H(16)	0.2700(4)	0.1266(3)	0.1095(6)	0.024(1)[b]
D(17)	−0.2820(3)	0.1026(2)	−0.0444(6)	0.0194(8)[b]
D(17)	−0.2626(3)	0.0942(2)	−0.0629(5)	0.0167(7)[b]
H(17)	−0.2628(4)	0.0944(3)	−0.0630(6)	0.022(1)[b]
D(18)	−0.1574(3)	0.1851(2)	0.0298(6)	0.0207(9)[b]
D(18)	−0.1346(3)	0.1850(2)	−0.0021(5)	0.0166(8)[b]
H(18)	−0.1335(4)	0.1854(3)	−0.0008(6)	0.022(1)[b]
D(19)	−0.0852(3)	−0.0630(2)	0.3335(6)	0.0198(8)[b]
D(19)	−0.1039(3)	−0.0557(2)	0.3172(5)	0.0176(8)[b]
H(19)	−0.1037(4)	−0.0557(3)	0.3170(6)	0.023(1)[b]
D(20)	0.0428(3)	−0.1395(2)	0.3168(5)	0.0166(8)[b]
D(20)	0.0208(3)	−0.1420(2)	0.3107(5)	0.0172(8)[b]
H(20)	0.0208(4)	−0.1421(2)	0.3103(6)	0.021(1)[b]

[a] Line 1: $(ND_4)_2[Cu(D_2O)_6](SO_4)_2$ at 15 K and 1 bar ($\mathbf{D_L}$). Line 2: $(ND_4)_2[Cu(D_2O)_6](SO_4)_2$ at 15 K and 1.5 kbar ($\mathbf{D_H}$). Line 3: $(NH_4)_2[Cu(H_2O)_6](SO_4)_2$ at 14 K and 1.5 kbar ($\mathbf{H_H}$). [b] Atom refined anisotropically, where $U_{eq} = {}^1/_3\sum_{ij}U_{ij}a_i^*a_j^*\mathbf{a}_i\cdot\mathbf{a}_j$.

(24) Jacobson, R. A. *J. Appl. Crystallogr.* **1986**, *19*, 283.
(25) Howard, J. A. K.; Johnson, O.; Schultz, A. J.; Stringer, A. M. *J. Appl. Crystallogr.* **1987**, *20*, 120.
(26) Main, P.; Fiske, S. J.; Hull, S. E.; Lessinger, L.; Germain, G.; Declercq, J.-P.; Woolfson, M. M. MULTAN80: A System of Computer Programs for the Automated Solutions of Crystal Structures from X-ray Diffraction Data. University of York, England, and University of Louvain, Belgium, 1980.
(27) Schultz, A. J.; Teller, R. G.; Beno, M. A.; Williams, J. M.; Brookhart, M.; Lamanna, W.; Humphrey, M. B. *Science* **1983**, *220*, 197.
(28) Schultz, A. J.; Hatton, P. D.; McMahon, M. I. S.; Nelmes, R. J. To be published.
(29) Sears, V. F. In *Neutron Scattering*; Sköld, K., Price, D. L., Eds.; Methods of Experimental Physics, Vol. 23; Academic Press: Orlando, FL, 1986; pp 521–550, Part A.
(30) Becker, P. J.; Coppens, P. *Acta Crystallogr.* **1974**, *A30*, 129.

Table III. Atomic Distances and Angles

atoms	D_L (15 K, 1 bar)	D_H (15 K, 1.5 kbar)	H_H (14 K, 1.4 kbar)	atoms	D_L (15 K, 1 bar)	D_H (15 K, 1.5 kbar)	H_H (14 K, 1.4 kbar)
Cu(1)–O(7)	2.022(2)	2.290(2)	2.272(2)	N(10)–H(13)	1.027(4)	1.035(3)	1.026(3)
Cu(1)–O(8)	2.310(2)	2.014(2)	2.005(2)	N(10)–H(14)	1.029(3)	1.038(3)	1.039(4)
Cu(1)–O(9)	1.966(3)	1.988(3)	1.979(2)	O(7)–H(15)	0.986(4)	0.973(4)	0.967(4)
S(2)–O(3)	1.474(5)	1.501(5)	1.489(4)	O(7)–H(16)	0.981(4)	0.981(4)	0.973(3)
S(2)–O(4)	1.481(5)	1.475(5)	1.466(4)	O(8)–H(17)	0.970(3)	0.997(4)	0.983(5)
S(2)–O(5)	1.502(4)	1.501(5)	1.476(4)	O(8)–H(18)	0.975(3)	0.983(4)	0.989(4)
S(2)–O(6)	1.498(6)	1.478(5)	1.486(4)	O(9)–H(19)	1.000(4)	0.986(3)	0.979(3)
N(10)–H(11)	1.033(3)	1.024(4)	1.018(4)	O(9)–H(20)	0.979(3)	0.991(3)	0.982(4)
N(10)–H(12)	1.024(3)	1.026(3)	1.017(4)				
			Bond Angles (deg)				
O(7)–Cu(1)–O(8)	87.58(8)	88.82(9)	88.83(7)	H(12)–N(10)–H(13)	109.4(3)	108.9(3)	108.7(3)
O(7)–Cu(1)–O(9)	89.79(10)	90.40(9)	89.28(7)	H(12)–N(10)–H(14)	108.8(3)	110.8(3)	110.7(3)
O(8)–Cu(1)–O(9)	89.05(9)	88.76(10)	88.78(7)	H(13)–N(10)–H(14)	107.3(3)	110.8(3)	110.7(3)
O(3)–S(2)–O(4)	110.3(3)	109.7(3)	109.8(2)	Cu(1)–O(7)–H(15)	113.9(3)	109.6(2)	109.4(2)
O(3)–S(2)–O(5)	108.9(3)	107.6(3)	108.4(3)	Cu(1)–O(7)–H(16)	118.1(3)	114.0(2)	114.0(3)
O(3)–S(2)–O(6)	110.3(3)	109.2(3)	108.6(2)	H(15)–O(7)–H(16)	108.1(3)	106.7(3)	107.5(4)
O(4)–S(2)–O(5)	108.6(3)	109.1(3)	109.3(2)	Cu(1)–O(8)–H(17)	119.1(3)	114.5(2)	114.7(2)
O(4)–S(2)–O(6)	109.9(3)	111.4(3)	110.7(3)	Cu(1)–O(8)–H(18)	111.8(2)	114.6(2)	113.9(2)
O(5)–S(2)–O(6)	108.8(3)	109.8(3)	110.0(2)	H(17)–O(8)–H(19)	105.0(3)	106.2(3)	106.8(4)
H(11)–N(10)–H(12)	112.0(3)	111.1(4)	110.1(4)	Cu(1)–O(9)–H(19)	112.8(2)	114.2(3)	114.2(3)
H(11)–N(10)–H(13)	109.8(2)	107.0(3)	108.1(3)	Cu(1)–O(9)–H(20)	117.3(3)	118.0(3)	118.3(2)
H(11)–N(10)–H(14)	109.4(3)	108.2(3)	108.6(3)	H(19)–O(9)–H(20)	106.0(3)	104.6(3)	105.1(3)
			Hydrogen-Bond (A–H···B) Distances (Å) and Angles (deg)				
O(7)–H(15)···O(15)				N(10)–H(11)···O(6)			
A···B	2.754(4)	2.841(4)	2.831(3)	A···B	2.907(3)	2.903(3)	2.872(2)
H···B	1.772(4)	1.888(4)	1.881(4)	H···B	1.881(3)	1.928(4)	1.906(5)
A–H···B	174.2(3)	165.8(3)	166.6(3)	A–H···B	172.1(3)	158.0(3)	157.3(3)
O(7)–H(16)···O(16)				N(10)–H(12)···O(3)			
A···B	2.791(4)	2.840(3)	2.827(2)	A···B	2.882(3)	2.990(3)	2.971(2)
H···B	1.813(4)	1.886(4)	1.879(3)	H···B	1.918(3)	2.020(4)	2.011(5)
A–H···B	174.0(3)	163.4(3)	163.9(3)	A–H···B	155.8(3)	156.5(3)	156.4(4)
O(8)–H(17)···O(14)				N(10)–H(13)···O(4)			
A···B	2.791(3)	2.693(3)	2.658(3)	A···B	2.911(4)		
H···B	1.821(3)	1.695(4)	1.675(4)	H···B	1.890(5)		
A–H···B	179.1(3)	178.9(3)	178.4(3)	A–H···B	172.1(3)		
O(8)–H(18)···O(16)				N(10)–H(13)···O(3)			
A···B	2.839(3)	2.732(3)	2.722(2)	A···B		2.900(3)	2.885(2)
H···B	1.866(4)	1.749(3)	1.734(3)	H···B		1.875(4)	1.870(3)
A–H···B	176.0(3)	177.4(3)	177.2(3)	A–H···B		170.7(3)	169.6(4)
O(9)–H(19)···O(5)				N(10)–H(14)···O(5)			
A···B	2.736(3)	2.742(3)	2.727(2)	A···B	2.865(3)	2.864(3)	2.846(2)
H···B	1.743(4)	1.767(4)	1.760(3)	H···B	1.869(3)	1.830(4)	1.811(4)
A–H···B	171.5(3)	169.1(3)	168.6(3)	A–H···B	161.8(3)	173.3(4)	173.6(3)
O(9)–H(20)···O(3)							
A···B	2.690(3)	2.707(3)	2.690(2)				
H···B	1.720(3)	1.726(3)	1.718(4)				
A–H···B	170.6(3)	169.8(4)	169.9(3)				

and 0.451(4) Å, respectively, whereas the *c* axis *increases* by 0.275(1) Å, such that the lattice parameters of D_H closely resemble those of H_H (Table I). Comparison of the D_L and D_H structures also shows that the long axis of the Jahn–Teller distortion has switched by 90°, such that the Cu–O(7) bond length increases from 2.022(2) to 2.290(2) Å and the Cu–O(8) bond length decreases from 2.310(2) to 2.014(2) Å (Table III). Another major difference between the D_L structure and both the D_H and H_H structures is a rotation of the ammonium cation, resulting in the formation of the N(10)–H(13)···O(3) hydrogen bond at the expense of the N(10)–H(13)···O(4) hydrogen bond (see Table III and Figure 2). Thus, in the D_H and H_H structures, O(4) is an acceptor for only one hydrogen bond rather than two in the D_L structure. This lack of competition should mean that the O(8)–H(17)···O(4) hydrogen bond is stronger in the D_H and H_H structures than in the D_L structure. In the discussion of the room-temperature structure of the hydrogenous salt, it was suggested[20] that hydrogen bonding to a water molecule increases its ligating power. Hence, the metal–ligand interaction along the Cu–O(8) direction should be somewhat stronger in the D_H and H_H structures than in the D_L structure, and this could provide the driving force for the longest Cu–O bond switching from this water molecule in the D_L structure to the O(7) water molecule in the D_H and H_H structures. The quantitative discussion below suggests that only a very minor change in the interaction of the $Cu(H_2O)_6^{2+}$ group with the lattice would be sufficient to cause the Jahn–Teller switch.

Comparison of the lattice parameters of the H_H structure at 14 K and 1.4 kbar with the X-ray structure of the hydrogenous salt at 123 K and ambient pressure[18] reveals a slight decrease in the *a* and *b* axes but no change in the *c* axis. There is also no significant change in the three Cu–O bond lengths, so that in this case the increase in pressure has little effect on the $Cu(H_2O)_6^{2+}$ group or its interaction with the lattice.

Jahn–Teller Coupling and the Cu(II) Coordination Geometry. Conventionally, the distorted geometry of a six-coordinate Cu(II) complex is described in terms of the vibronic coupling between the ^2E_g electronic state and the e_g Jahn–Teller-active vibrational mode of the parent octahedral complex.[31] This suggests that to first order, a complex with six identical ligands will undergo a radial distortion in the e_g mode to yield the "Mexican hat" potential energy surface pictured in Figure 4A. At this level of approximation, the Q_θ and Q_ϵ components of the e_g vibration, pictured in Figure 4B, are equivalent and the energy minimum is a circular trough of radius ρ. If the position of the complex in this trough

(31) For a recent review of the Jahn–Teller effect in transition-metal chemistry see: Reinen, D.; Atanasov, M. *Magn. Reson. Rev.* **1991**, *15*, 167.

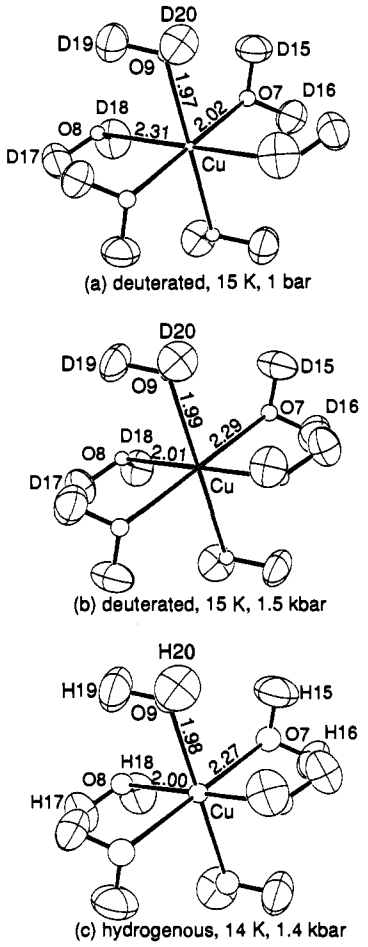

Figure 1. Coordination sphere around the copper atoms viewed parallel to the crystallographic *b* axes in (a) $(ND_4)_2[Cu(D_2O)_6](SO_4)_2$ at T = 15 K, P = 1 bar (D_L), (b) $(ND_4)_2[Cu(D_2O)_6](SO_4)_2$ at T = 15 K, P = 1.5 kbar (D_H), and (c) $(NH_4)_2[Cu(H_2O)_6](SO_4)_2$ at T = 14 K, P = 1.4 kbar (H_H). Note the switch in the Cu–O(7) and Cu–O(8) bond lengths between (a) and (b). Atoms are drawn at the 90% probability level.

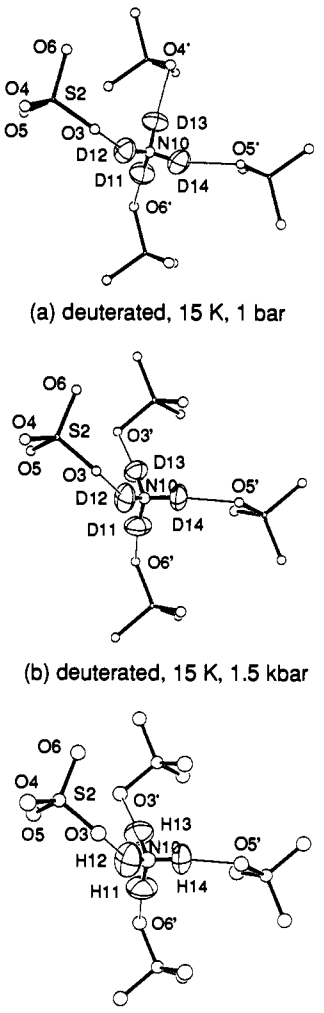

Figure 2. Hydrogen bonds between ammonium cations and sulfate anions in (a) $(ND_4)_2[Cu(D_2O)_6](SO_4)_2$ at T = 15 K, P = 1 bar (D_L), (b) $(ND_4)_2[Cu(D_2O)_6](SO_4)_2$ at T = 15 K, P = 1.5 kbar (D_H), and (c) $(NH_4)_2[Cu(H_2O)_6](SO_4)_2$ at T = 14 K, P = 1.4 kbar (H_H). Note that D(13) hydrogen bonds to O(4′) in (a) and to O(3′) in (b). Atoms are drawn at the 90% probability level.

is defined by an angle Φ, the ligand coordination geometry is given by the relationships $Q_\theta = \rho \cos \Phi$ and $Q_\epsilon = \rho \sin \Phi$ with $\rho = \{2[(\delta x)^2 + (\delta y)^2 + (\delta z)^2]\}^{1/2}$, where δx, δy, and δz are the deviations from the mean value of the metal–ligand bond lengths along the Cartesian axes. It may be noted that the present results show that the Jahn–Teller radius of $(ND_4)_2[Cu(D_2O)_6](SO_4)_2$ decreases slightly on going from 1 bar (D_L, ρ = 0.368 Å) to 1.5 kbar (D_H, ρ = 0.335 Å). Comparison of the X-ray data at 123 K and 1 bar (ρ = 0.334 Å)[18] with the present results at 1.4 kbar (H_H, ρ = 0.324 Å) suggests that a similar effect occurs for the hydrogenous salt; moreover, the Jahn–Teller radius of the hydrogenous salt is somewhat smaller than that of the deuterated salt.

Higher-order effects stabilize the elongated form of the Q_θ component of the e_g mode and destabilize the compressed form, thus "warping" the Mexican hat potential surface to give three equivalent minima at Q_θ = 0, 120, and 240°. When a Cu(II) complex occupies a lattice site of orthorhombic or lower symmetry, the minima in the warped Mexican hat potential surface shift from the above positions and their energies become nonequivalent. This occurs in the potential surfaces of the Tutton salts, where the Cu^{2+} ions occupy a site of $\bar{1}$ symmetry in a monoclinic lattice.

The nature of the potential surfaces in the Tutton salts was first investigated quantitatively by Silver and Getz[5] in an interpretation of the temperature dependence of the EPR spectrum of Cu^{2+} doped into $K_2[Zn(H_2O)_6](SO_4)_2$. It was observed that as the temperature increases, the two higher molecular g values of the $Cu(H_2O)_6^{2+}$ guest complex converge. This was explained in terms of an equilibrium between two structural isomers differing in the orientation of the long and intermediate Cu–O bond directions and separated in energy by ≈75 cm^{-1}. This basic model was subsequently applied to explain the temperature-dependent EPR spectra of Cu^{2+} doped into a range of other Tutton salts,[6] as well as to the apparent variation of the metal–ligand bond lengths observed by X-ray diffraction for various Cu(II) complexes[11,12] including $(NH_4)_2[Cu(H_2O)_6](SO_4)_2$.[18] A similar pattern was revealed in a study of the temperature dependence of the structure of $(ND_4)_2[Cu(D_2O)_6](SO_4)_2$ by powder neutron diffraction,[19a] where it was also noted that the shifts in apparent Cu–O bond lengths are accompanied by changes in the hydrogen-bonding network in the lattice. It must be stressed that this model suggests that the coordination geometry about each Cu^{2+} ion is always of the normal, tetragonally elongated form and that the apparent change toward a tetragonally compressed geometry at higher temperatures occurs because the bond lengths revealed by diffraction experiments are the *average* of those of the two structural isomers weighted by their Boltzmann population factors.

A more detailed model to describe these "fluxional" Cu(II) complexes was developed by Riley et al. to interpret the

(32) Riley, M. J.; Hitchman, M. A.; Reinen, D.; Steffen, G. *Inorg. Chem.* **1988**, *27*, 1924. Steffen, G.; Reinen, D.; Stratemeier, H.; Riley, M. J.; Hitchman, M. A.; Matthies, H. E.; Recker, K.; Wallrafen, F.; Niklas, J. R. *Inorg. Chem.* **1990**, *29*, 2123.

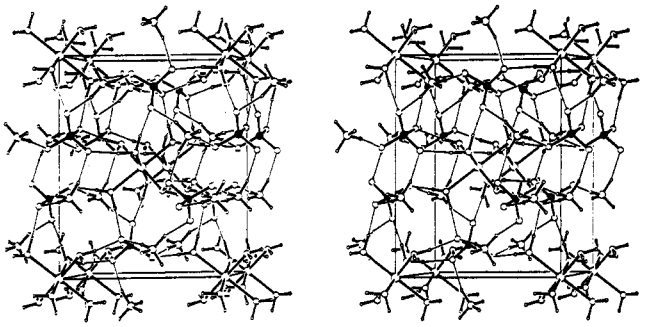

(a) deuterated, 15 K, 1 bar

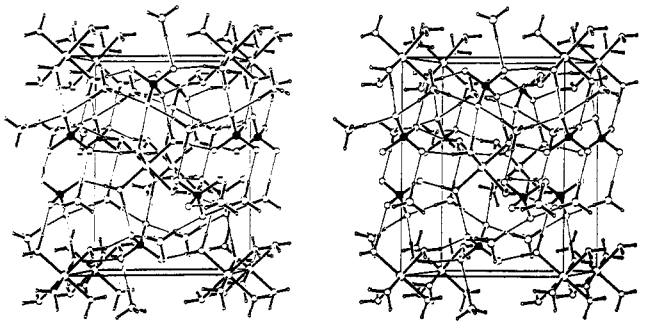

(b) deuterated, 15 K, 1.5 kbar

Figure 3. Stereoviews of the unit cell packing of (a) $(ND_4)_2[Cu(D_2O)_6](SO_4)_2$ at T = 15 K, P = 1 bar (D_L) and (b) $(ND_4)_2[Cu(D_2O)_6](SO_4)_2$ at T = 15 K, P = 1.5 kbar (D_H). The a axes are horizontal, and the b axes are vertical. Atoms are drawn with arbitrary sizes (Cu > S, N > O > H) for clarity. Sulfur atoms are filled, and hydrogen bonds are shown as thin lines.

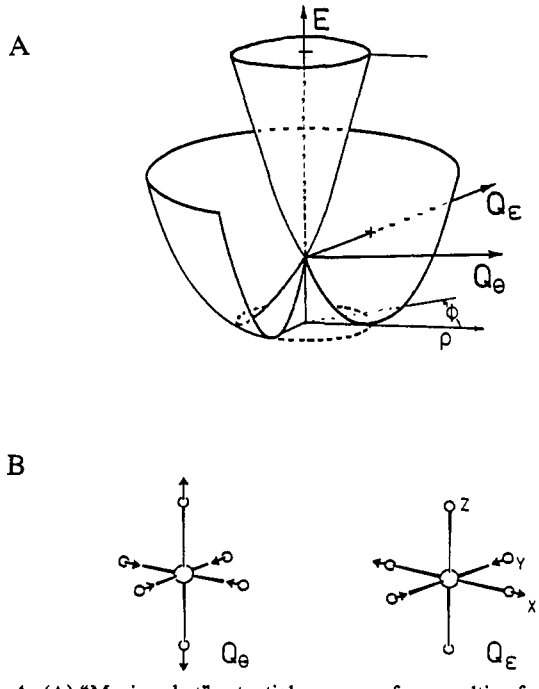

Figure 4. (A) "Mexican hat" potential energy surface resulting from $E_g \times e_g$ vibronic coupling. (B) Form of the two components of the Jahn–Teller-active e_g vibration.

temperature-dependent EPR parameters of Cu^{2+} doped into a range of host lattices,[8,32] including a number of Tutton salts.[9] This approach, described in detail elsewhere,[8,9] calculates the vibronic energy levels of the complexes by applying Jahn–Teller coupling (defined by a linear coupling constant A_1) plus a "warping" interaction (described by a second-order coupling constant A_2) to a basis set consisting of the $d_{x^2-y^2}$ and d_{z^2} electronic wave functions, and harmonic oscillator vibrational wave functions of the first 40 levels of the e_g vibration, with a lattice strain consisting of tetragonal and orthorhombic components S_θ and S_ϵ, respectively, included. The g values of each complex are estimated from the electronic parts of the eigenfunctions of the calculation, with the temperature dependence being given by the changes in the Boltzmann populations of the energy levels. The model was recently extended to allow for the calculation of the temperature variation of the time-averaged molecular geometry from the vibrational part of each eigenfunction.[33] The minor changes in procedure necessary to do this involve a Boltzmann summation of the Q_θ and Q_ϵ components of the e_g mode associated with each energy level to yield temperature-dependent nuclear probability functions, which are then converted into apparent bond length changes.

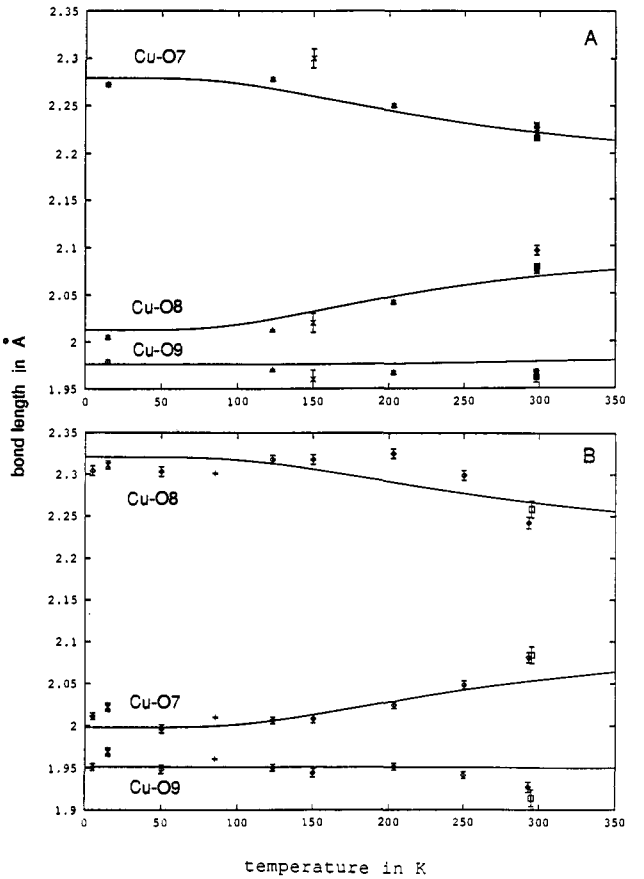

Figure 5. Variation of the Cu–O bond lengths as a function of temperature reported for (A) $(NH_4)_2[Cu(H_2O)_6](SO_4)_2$ and (B) $(ND_4)_2[Cu(D_2O)_6](SO_4)_2$. The sources of the data are as follows: (A) (◇) this paper, (□) ref 20 (neutron), (○) ref 20 (X-ray), (△) ref 18, (*) ref 16, (×) Duggan, M.; Murphy, A.; Hathaway, B. J. *Inorg. Nucl. Chem. Lett.* **1979**, *15*, 103; (B) (◇) ref 19a, (□) ref 38, (+) ref 19b, (×) this paper. The calculated curves were derived using the parameters (in cm^{-1}) A_1 = 900, S_θ = –400, and S_ϵ = 170 for (A) and A_1 = 1100, S_θ = –600, and S_ϵ = –200 for (B) with A_2 = 33 (corresponding to a warping parameter β = 300; the energy differences between the minima and maxima of the warped Mexican hat potential surface of the complex unperturbed by the lattice strain would be 2β). The energy of the e_g vibration = 300 for both complexes.

Using the extended model, we have calculated the temperature variations of the Cu–O bond lengths in the D_L and H_H structures; Figure 5 shows a comparison of the bond lengths with those observed experimentally by X-ray and/or neutron diffraction. In the calculation, x, y, and z were defined along the Cu–O(8),

(33) Stratemeier, H.; Hitchman, M. A.; Bebendorf, J.; Reinen, D.; Gamp, E.; Bürgi, H. B. To be published.

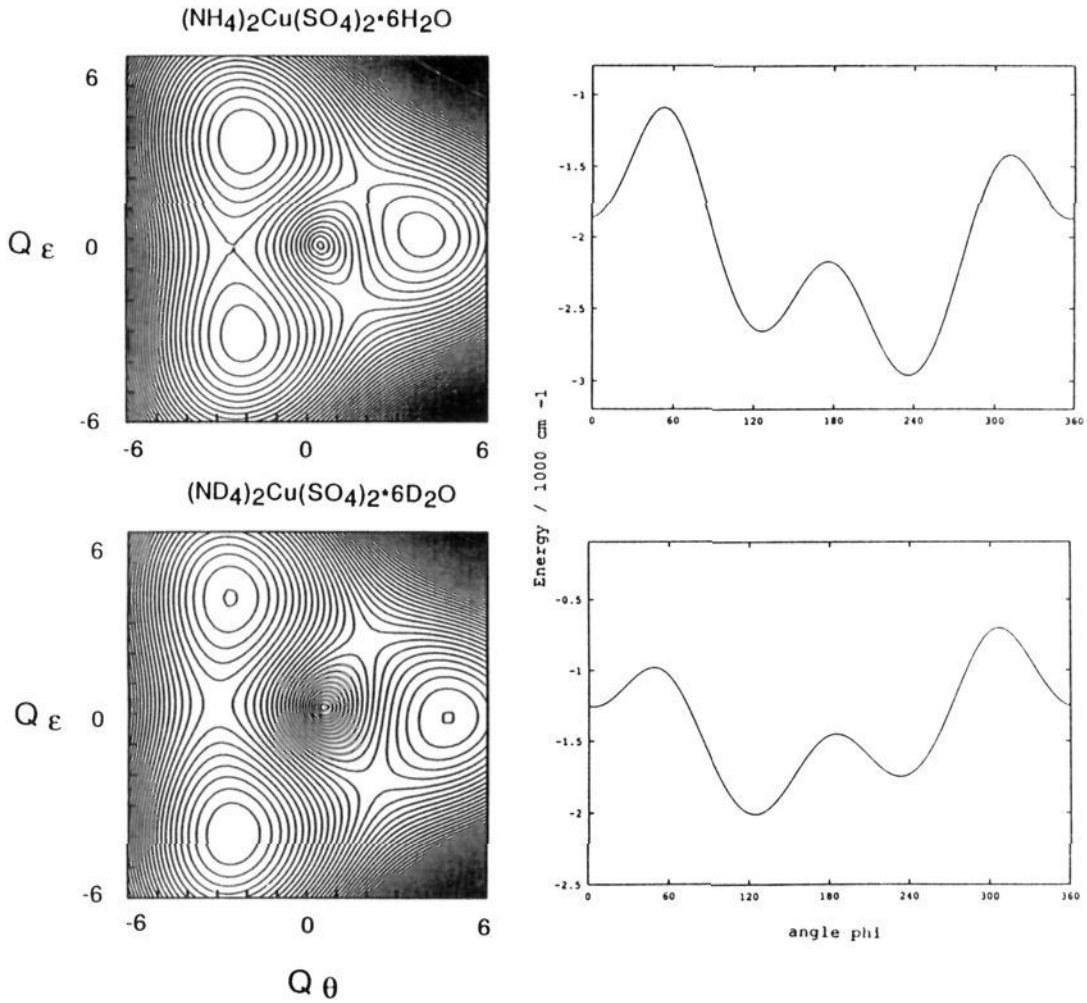

Figure 6. Left: Energy contour plots of the lower region of the Mexican hat potential surface of the complexes (the spacing between each pair of curves represents 120 and 110 cm^{-1} for the hydrogenous and deuterated salts, respectively). Right: Variation of the potential energy as a function of coordination geometry at a fixed Jahn–Teller radius, equal to that in the potential energy minimum (see text for the relationship between the coordination geometry and the angle Φ).

O(7), and O(9) directions, respectively. The parameters used in the calculations were those used previously[9] to fit the temperature dependence of Cu^{2+} doped into $(NH_4)_2[Zn(H_2O)_6](SO_4)_2$, and apart from the lattice strain parameters, these give reasonable agreement with experiment, except that a slightly higher value of the linear coupling constant A_1 was used for $\mathbf{D_L}$ (1100 cm^{-1} compared with 900 cm^{-1}). For the $\mathbf{D_L}$ structure, the bond length changes deviate somewhat from the predictions of the model at higher temperatures. Such behavior, which is also apparent in the g values of the pure compound, implies that the potential surface is somewhat temperature dependent, possibly due to cooperative interactions and/or changes in the hydrogen-bonding network.[34]

Contour energy plots of the Mexican hat potential energy surfaces of the $Cu(H_2O)_6^{2+}$ group in the two compounds, viewed from above, are shown on the left side of Figure 6. The three energy minima are clearly evident in the plots; they are similar except for a difference of $\approx 120°$ in Φ for the lowest energy well, corresponding to the long Cu–O axis oriented along y for the $\mathbf{H_H}$-hydrogenous salt and x for the $\mathbf{D_L}$-deuterated salt. The variations of the potential energies as a function of Φ at the Jahn–Teller radii of the energy minima are pictured on the right side of Figure 6. (It should be noted that these plots do not represent the lowest energy pathway between the minima, as this does not follow a circle of constant Jahn–Teller radius.) Although all the vibrational functions below 1000 cm^{-1} were used in the calculations, in both cases the results are dominated by the first two energy levels. To a good approximation, these correspond to the complex being localized in the two lower wells, with a similar orthorhombic geometry occurring in each, but with the orientation of the long and intermediate Cu–O bond directions being switched. For the $\mathbf{H_H}$-hydrogenous salt, the energy separation between the two levels is 247 cm^{-1}, while for the deuterated it is 250 cm^{-1}, with the ordering of the wells switched between the two compounds. Thus, the simple Silver–Getz model provides a good approximation for the present compounds, and the energy separation derived previously[4] using this approach for the hydrogenous compound (160 cm^{-1}) agrees moderately well with that of the present study. As noted previously,[9] the relative energy of the two lower wells is decided largely by the sign and magnitude of the orthorhombic component of the strain, S_ϵ.

The lattice strain parameters used for the plots in Figures 5 and 6 are for $\mathbf{H_H}$, $S_\theta = -400$ cm^{-1} and $S_\epsilon = 170$ cm^{-1} and, for $\mathbf{D_L}$, $S_\theta = -600$ cm^{-1} and $S_\epsilon = -200$ cm^{-1} (a negative sign of S_θ corresponds to compression). The values for the protonated salt are similar to those deduced[9] from the analysis of the EPR spectrum of Cu^{2+} doped into $(NH_4)_2[Zn(H_2O)_6](SO_4)_2$ ($S_\theta = -550$ cm^{-1} and $S_\epsilon = 120$ cm^{-1}). It is instructive to estimate the distortions such strains would induce in a regular octahedral $Cu(H_2O)_6^{2+}$ group in the absence of the Jahn–Teller effect. Taking

(34) Stratemeier, H.; Hitchman, M. A.; Reinen, D.; Maaskant, W. J. To be published.

the energy of the e_g mode as 300 cm^{-1} (energies of 305 and 278 cm^{-1} have been reported for the corresponding Ni^{2+} and Zn^{2+} complexes, respectively[35]) yields the following estimates (in Å): H_H, $\delta x = 0.003$, $\delta y = 0.018$, $\delta z = -0.020$; D_L, $\delta x = 0.020$, $\delta y = 0.005$, $\delta z = -0.025$. Thus, the estimated strain parameters predict a shortening of the metal–ligand bond along the z direction, accompanied by an unequal lengthening along x and y. Moreover, while $\delta x < \delta y$ in the hydrogenous salt, the reverse is true in the deuterated compound. These shifts from the mean bond length may be compared with those observed for the corresponding Zn(II) compounds: H-salt,[36] $\delta x = 0.014$, $\delta y = 0.017$, $\delta z = -0.030$; D-salt,[37] $\delta x = 0.013$, $\delta y = 0.015$, $\delta z = -0.029$. The overall pattern observed for the non-Jahn–Teller-active Zn(II) compounds is similar to that estimated using the Cu(II) strain parameters, except that the difference between δx and δy is smaller, and apparently does not change sign on going from the hydrogenous to the deuterated compound (this is confirmed[38] by the EPR spectrum of Cu^{2+} doped into $(ND_4)_2[Zn(D_2O)_6](SO_4)_2$).

Implications of the Strain Parameters on the Pressure-Dependent Jahn–Teller "Switch" of $(ND_4)_2[Cu(D_2O)_6](SO_4)_2$. The temperature dependence of the structure of $(ND_4)_2[Cu(D_2O)_6](SO_4)_2$ shows that the higher energy form of this compound, in which the lengths of the Cu–O(7) and Cu–O(8) bonds interchange, lies only ≈250 cm^{-1} above the more stable form. The key parameter deciding the relative stability of the two forms is apparently the nonequivalence of the lattice strain acting along these two bond directions, S_ϵ. A quite small value of S_ϵ, sufficient to cause bond length differences of ≈0.02 Å in the absence of Jahn–Teller coupling, is greatly amplified by this effect, so that the deviations (in Å) of bond lengths from their mean in the D_L structure are $\delta x = 0.211(2)$, $\delta y = -0.077(2)$, and $\delta z = -0.133(3)$.

The change in structure which occurs for the above compound at 1.5 kbar may be explained if S_ϵ changes sign at high pressure, becoming similar to that of the hydrogenous complex. As already mentioned, this alteration in lattice strain appears to be associated with a change in the hydrogen-bonding pattern in the lattice, though why this should differ when deuterium replaces hydrogen remains unclear. This picture suggests that the high-pressure form of the deuterated complex may well exhibit a temperature-dependent structural equilibrium like that of the hydrogenous compound at 1 bar of pressure, and preliminary results suggest that this is indeed the case.[38] It is not yet clear whether the lattice strain alters gradually as the pressure increases or changes sharply at a particular pressure. However, the fact that the structure varies continuously with temperature implies that the lattice strain may vary smoothly with pressure, and we are currently investigating this aspect.

Acknowledgment. Work at Argonne National Laboratory is sponsored by the Office of Basic Energy Sciences, Division of Materials Sciences, U.S. Department of Energy, under Contract W-31-109-ENG-38. C.J.S. acknowledges travel funds provided by BYU-HI; M.A.H. and H.S. acknowledge financial assistance from the Australia Research Commission.

Supplementary Material Available: Tables of anisotropic thermal parameters for $(ND_4)_2[Cu(D_2O)_6](SO_4)_2$ (3 pages); tables of neutron structure factors for $(ND_4)_2[Cu(D_2O)_6](SO_4)_2$ (17 pages). Ordering information is given on any current masthead page.

(35) Jenkins, T. E.; Lewis, J. *Spectrochim. Acta, Part A* **1981**, *37*, 47.
(36) Maslen, E. N.; Watson, K. J.; Ridout, S. C. *Acta Crystallogr., Sect. C* **1988**, *44*, 1510.
(37) Hitchman, M. A.; Stratemeier, H.; Massa, W. To be published.
(38) Asbahs, H.; Rauw, W.; Reinen, D.; Hitchman, M. A. To be published.